available at www.sciencedirect.com
journal homepage: www.europeanurology.com

European Association of Urology

Platinum Priority – Urothelial Cancer

Editorial by Lars Dyrskjøt on pp. 433–434 of this issue

Molecular Subtypes of Urothelial Bladder Cancer: Results from a Meta-cohort Analysis of 2411 Tumors

Tuan Zea Tan [a,*], *Mathieu Rouanne* [b,c], *Kien Thiam Tan* [d], *Ruby Yun-Ju Huang* [a,e,f,*], *Jean-Paul Thiery* [g,h,i,j]

[a] *Cancer Science Institute of Singapore, National University of Singapore, Center for Translational Medicine, Singapore;* [b] *Department of Urology, Hôpital Foch, Université Versailles-Saint-Quentin-en-Yvelines, Université Paris-Saclay, Suresnes, France;* [c] *INSERM Unit 1015, Laboratoire de Recherche Translationnelle en Immunologie (LRTI), Gustave Roussy, Université Paris-Saclay, Villejuif, France;* [d] *ACT Genomics Co., Ltd., Taipei city, Taiwan;* [e] *Department of Obstetrics and Gynecology, National University Health System, Singapore;* [f] *Department of Anatomy, Yong Loo Lin School of Medicine, National University of Singapore, Singapore;* [g] *Biochemistry Yong Loo Lin School of Medicine, National University of Singapore, Singapore;* [h] *Guangzhou Institute of Biomedicine and Health, Chinese Academy of Science, Guangzhou, People's Republic of China;* [i] *CNRS Emeritus CNRS UMR 7057 Matter and Complex Systems, University Paris Denis Diderot, Paris, France;* [j] *INSERM UMR 1186, Integrative Tumor Immunology and Genetic Oncology, Gustave Roussy, EPHE, PSL, Fac. de Médecine - University Paris-Sud, Université Paris-Saclay, Villejuif, France*

Article info

Article history:
Accepted August 16, 2018

Associate Editor:
James Catto

Keywords:
Bladder carcinoma
Microarray gene expression
Molecular subtypes

Abstract

Background: Previous molecular subtyping for bladder carcinoma (BLCA) involved <450 samples, with diverse classifications.
Objective: To identify molecular subtypes by curating a large BLCA dataset.
Design, setting, and participants: Gene expression publicly available were combined and reanalyzed. The dataset contained 2411 unique tumors encompassing non-muscle-invasive (NMIBC) and muscle-invasive BLCA (MIBC). Subtypes were reproduced on The Cancer Genome Atlas, UROMOL, and IMvigor210.
Intervention: Subtypes were assigned by gene expression.
Outcome measurements and statistical analysis: Kaplan-Meier analyses were performed for subtype-clinical outcome correlations; Chi-square/Fisher exact tests were used for subtype-clinicopathological parameters associations.
Results and limitations: We identified six molecular subtypes with different overall survival (OS) and molecular features. Subtype Neural-like (median OS, 87 mo) is prevalent in MIBC and characterized by high WNT/β-catenin signaling. HER2-like (107.7 mo) is distributed evenly across NMIBC and MIBC, with higher *ERBB2* amplification and signaling. Papillary-like (>135 mo), an NMIBC subtype enriched in urothelial differentiation genes, shows a high frequency of actionable *FGFR3* mutations, amplifications, and *FGFR3-TACC3* fusion. Luminal-like (91.7 mo), predominantly NMIBC, has higher MAPK signaling and more *KRAS* and *KMT2 C/D* mutations than other subtypes. Mesenchymal-like (MES; 86.6 mo) and Squamous-cell carcinoma-like (SCC; 20.6 mo) are predominant in MIBC. MES is high in AXL signaling, whereas SCC has elevated PD1, CTLA4 signaling, and macrophage M2 infiltration. About 20% of NMIBCs show MIBC subtype traits and a lower 5-yr OS rate than Papillary-like NMIBC (81% vs 96%). The main limitations of our study are the incomplete clinical annotation, and the analyses were

* Corresponding authors. Cancer Science Institute (T.Z. Tan and R.Y.-J. Huang) and Department of Biochemistry (J.-P. Thiery) Yong Loo Lin School of Medicine, National University of Singapore, 8 Medical Drive, Blk MD7, #02-03, Singapore 117597. Tel. +65 6516 1148 (T.Z. Tan and R.Y.-J. Huang) and +65 6516 3242 (J.-P. Thiery); Fax: +65 6516 1453.
E-mail addresses: csittz@nus.edu.sg (T.Z. Tan), bchtjp@nus.edu.sg (J.-P. Thiery).

https://doi.org/10.1016/j.eururo.2018.08.027

based on transcriptome subset due to comparisons across gene expression quantification technologies.
Conclusions: BLCA can be stratified into six molecular subtypes. NMIBC, with a high risk of progression, displays the molecular features of MIBC.
Patient summary: Biomarkers are urgently needed to guide patient treatment selection and avoid unnecessary toxicities in those who fail to respond. We believe molecular subtyping is a promising way to tailor disease management for those who will benefit most.

1. Introduction

Bladder carcinoma (BLCA) is one of the most common and lethal diseases worldwide, with approximately 430 000 new cases and more than 165 000 related deaths per year [1], a figure anticipated to double in the near future [2]. Urothelial carcinoma (UC) is the predominant histological type, with less-frequent histological variants including squamous (Squa), glandular differentiation (GD), neuroendocrine (NE), micro-papillary (MP), sarcomatoid, (Sarco) and plasmocytoid tumors. At diagnosis, 75% of patients have non–muscle-invasive BLCA (NMIBC), whereas the remaining 25% have muscle-invasive BLCA (MIBC) [2]. NMIBC is characterized by common activating *FGFR3* mutations, diploid or near-diploid karyotypes, frequent recurrence (50–70%) but a low propensity to progress (10–15%), and a 5-yr survival of ~90% [2,3]. MIBC, however, is characterized by frequent *TP53* mutations, aneuploidy, with many chromosomal alterations, high rates of metastasis, and a 5-yr survival of <50% despite radical surgery [4].

On the therapeutic front, the management is distinct for NMIBC and MIBC. The treatment has remained essentially unchanged over the past few decades [3] until the launch of clinical trials using fibroblast growth factor receptor (FGFR)-targeting agents [5] and the US Food and Drug Administration approval of immune checkpoint inhibitors [6,7] in first-line or metastatic settings. However, most patients do not benefit from these cancer therapies. The IMvigor210 phase II trial in platinum-treated locally advanced UC reported that the molecular subtype proposed by The Cancer Genome Atlas (TCGA) was associated with atezolizumab clinical response [8,9]. This suggests that stratification of BLCA based on molecular subtype could be an effective strategy for therapeutic regimen allocation.

Apart from TCGA [10,11], several studies have shown that NMIBC and MIBC could be assigned across 2–7 molecular subtypes based on transcriptomic [12–16] or genomic [17] data and with distinct clinicopathological characteristics. To facilitate clinical adoption, a consensus classification unifying these different subtypes is needed. Attempts have been made to unravel the complexity and refine these molecular subtypes [16,18–20] based on biomarkers and pathways, mutations and copy number aberrations, or protein abundance [21]. Motivated by the need for a unifying subtype scheme, in this original study, we collated and analyzed a collection of 2411 BLCA gene expression profiles. Such a large sample size allows for greater statistical power in subtype identification and characterization, and minimizes sampling bias [22]. This study is also motivated by one of the most important unmet clinical needs of identifying potentially lethal NMIBCs. These NMIBCs, with a very high risk of disease progression, can be subjected to more aggressive disease management [23]. As high-risk NMIBC may display MIBC traits [14,17], NMIBC and MIBC tumors were analyzed together in this meta-cohort to allow for comparisons between the two progression pathways at the molecular level.

2. Materials and methods

2.1. Inclusion criteria

We adopted broad inclusion criteria because the aim of the study was to compile a database for broader generalization (covering different stages, grades, and histologies) and for a larger sample size [24]. All publicly available data annotated as BLCA were included (last accessed May 4, 2018). Clinical data of GSE38264 [25] was kindly provided by the authors.

2.2. Gene expression analysis

We downloaded the publicly available BLCA gene expression datasets (Supplementary Fig. 1; Supplementary data). A total of 36 cohorts were collected. Cohorts with <20 tumors and cohorts hybridized on older (Affymetrix U133A) or two-color microarray platforms were removed from meta-cohort compilation (Supplementary Tables 1 and 2; Supplementary data). We performed a quality check, platform-specific normalization, and combined them by ComBat [26] (Supplementary Fig. 2; Supplementary data). Duplicate samples were removed from the meta-cohort (Supplementary Table 3). Principal component analysis, clinicopathological parameter correlations, and batch effect metrics [27] assessment were performed to ensure minimization of batch effect (Supplementary Fig. 2; Supplementary data). Validation RNA-seq datasets—TCGA BLCA version 2016_01_28 [28], UROMOL E-MTAB-4321, and IMvigor210—were downloaded from GDAC, ArrayExpress, and the Supplementary data of Mariathasan et al. [9], respectively. Significantly mutated genes and focal copy number aberrations were extracted from Robertson et al. [11], and the distribution of these mutations and aberrations was analyzed.

We employed the R ConsensusClusterPlus v1.36.0 [29] to identify clusters in the meta-cohort using the most varying 5328 genes out of the 10596 genes common across the expression microarray platforms (Supplementary data). Core samples were defined by silhouette width of >0.01. Previously reported subtypes were inferred by the published predictor [30] or consensus clustering using subtype signatures [15,20,21]. We employed an epithelial-mesenchymal transition projection [31] and R GSVA 1.20.0 to estimate pathway enrichment scores for each sample. Immune cell infiltration was estimated using CIBERSORT [32].

2.3. Statistical analysis

Statistical tests were computed using Matlab R2016b (MathWorks; Natick, MA, USA). Kaplan-Meier analyses were computed using

GraphPad Prism v5.04 (GraphPad Software; La Jolla, CA, USA). Differences in the mean expression or pathway enrichment scores between subtypes were computed using Significant Analysis of Microarray (SAM, software website, https://github.com/MikeJSeo/SAM) or analysis of variance test. Subtype association analyses of clinical parameters were computed using chi-square/Fisher exact tests. Correlation analyses were computed using the Spearman's rank correlation coefficient test.

3. Results

3.1. UC meta-cohort shows six molecular subtypes, displaying good overlap with published subtypes

To identify molecular subtype based on gene expression, we compiled a BLCA meta-cohort of 2411 samples from 19 UC cohorts and applied a consensus clustering algorithm [29] (Table 1; Supplementary Table 1; Supplementary Figs. 1–4; Supplementary data). Based on similarity matrix, change in the area under the curve value, and sample cluster consensus metrics, we selected a stable classification of six major molecular subtypes (MC1–6; $n > 100$ in each cluster; Fig. 1A; Supplementary Fig. 3), hereafter denoted as "BOLD" for BLCA subtypes Of Large meta-cohort Database. To ensure that BOLD did not result from potential confounding factors (eg. batch effect, tissue source), we checked the distribution of BOLD across different clinical parameters, tissue sources, cohorts, and microarray platforms (Supplementary Fig. 3D; Supplementary Table 4). All six subtypes were distributed evenly across clinicopathological parameters, cohorts, and gene expression microarray platforms. We labeled several genes implicated in BLCA subtyping, such as basal, luminal, immune, proliferation, differentiation, and other subtype markers previously reported [16,20,21] (Fig. 1; Supplementary Table 9).

To investigate if BOLD subtypes overlapped with published subtypes, we adopted a three-pronged strategy to compare BOLD against published subtypes (Supplementary data). First, we checked the markers expressed in each subtype (Fig. 1A; Supplementary Tables 8 and 9). Second, we extracted the existing subtype annotation (Supplementary Fig. 5A). Third, we re-performed consensus clustering on a subset of the BLCA meta-cohort (selected by microarray platform) using most varying genes and published subtype signatures [10,13–15,30], and then annotated the samples with published subtypes based on biomarkers or predictor outputs (Fig. 1B and 1C; Supplementary Fig. 5B; Supplementary data). The three-pronged strategy yielded accordant results that BOLD has good agreement with published subtypes (Supplementary Fig. 5C; Supplementary data). We annotated the BOLD MC1-6 with selected biological features (Fig. 1D): MC1/Neural-like (NEURAL) is similar to LUND_SC/NE and TCGA_Neuronal subtypes; MC2/Luminal-like (LUM) is most similar to UROMOL2016_C3; MC3/Papillary-like (PAP) to LUND_Urobasal (Uro)/TCGA_Luminal-papillary; MC4/HER2-like (HER2L) to LUND_Genomic Unstable (GU)/TCGA_Luminal; MC5/Squamous-cell carcinoma-like (SCC) to LUND_ SCC-like)/MDA_basal/TCGA_Basal-Squamous; and MC6/Mesenchymal-like (MES) to LUND_Infiltrated (Inf)/MDA_TP53/TCGA_Luminal-infiltrated. UNC_Luminal encapsulated HER2L, LUM, and PAP, whereas basal captured NEURAL, MES, and SCC (Fig. 1D). Compared with published NMIBC subtypes (Fig. 1C and 1D), the HER2L, MES, and SCC subtypes were similar to the aggressive genomic subtype LICAP_HG2 [17], and paradoxically, PAP was akin to LICAP_HG1 ($p = 5.3E-27$; Fig. 1C). Similarly, we observed the poor prognosis of HER2L and SCC subtypes enriched in the aggressive, MIBC-like UROMOL2016_C2 [33]. However, LUM was enriched in another aggressive UROMOL2016_C3 [33] ($p = 3.2E-155$; Fig. 1C).

Table 1 – Clinical information of urothelial carcinoma meta-cohort

	n	%
No. of cohorts	19	100
No. of samples	2533	100
Normal	122	4.82
Primary	2388	94.58
Recurrent	23	0.91
Histology		
Urothelial carcinoma (with CIS)	1973 (37)	81.8 (1.5)
Micropapillary	53	2.2
Squamous/epidermoid	46	1.91
Sarcomatoid	6	0.25
Glandular/adenocarcinoma/lymphoepithelioma	6	0.25
Neuroendocrine/small cell	6	0.25
Mixed/other	5/9	0.21/0.37
Not available	307	12.73
Gender		
Male	797	33.07
Female	225	9.33
Not available	1,389	57.61
Age		
Median (yr)	67	–
Min–max	20–96	–
Muscle-invasive		
Yes	1386	57.49
No	653	27.08
Not available	372	15.43
Stage[a]		
pTa/pT1	678	26.77
pT2	579	22.86
pT3/pT4	440	17.37
Not available	580	24.06
Lymph node invasion		
No	596	24.72
Yes	143	5.93
Not available/not applicable	1226/446	50.9/18.5
Metastasis		
Loco-regional	622	25.79
Distant	88	3.65
Not available/not applicable	1235/466	51.2/19.3
Overall survival		
Median (mo)	35.35	–
No. of events	347	14.39
Disease-free survival		
Median (mo)	18.99	–
No. of events	49	2.03
Grade		
Low[b]	331	13.73
High	828	34.34
Not available	1252	51.93
Surgery		
Cystectomy	414	17.17
Transurethral resection	992	41.15
Not available	1005	41.68

CIS = carcinoma in situ.
[a] pT0, Tx excluded.
[b] Combined with 130 (5.4%) originally labeled punlump samples.

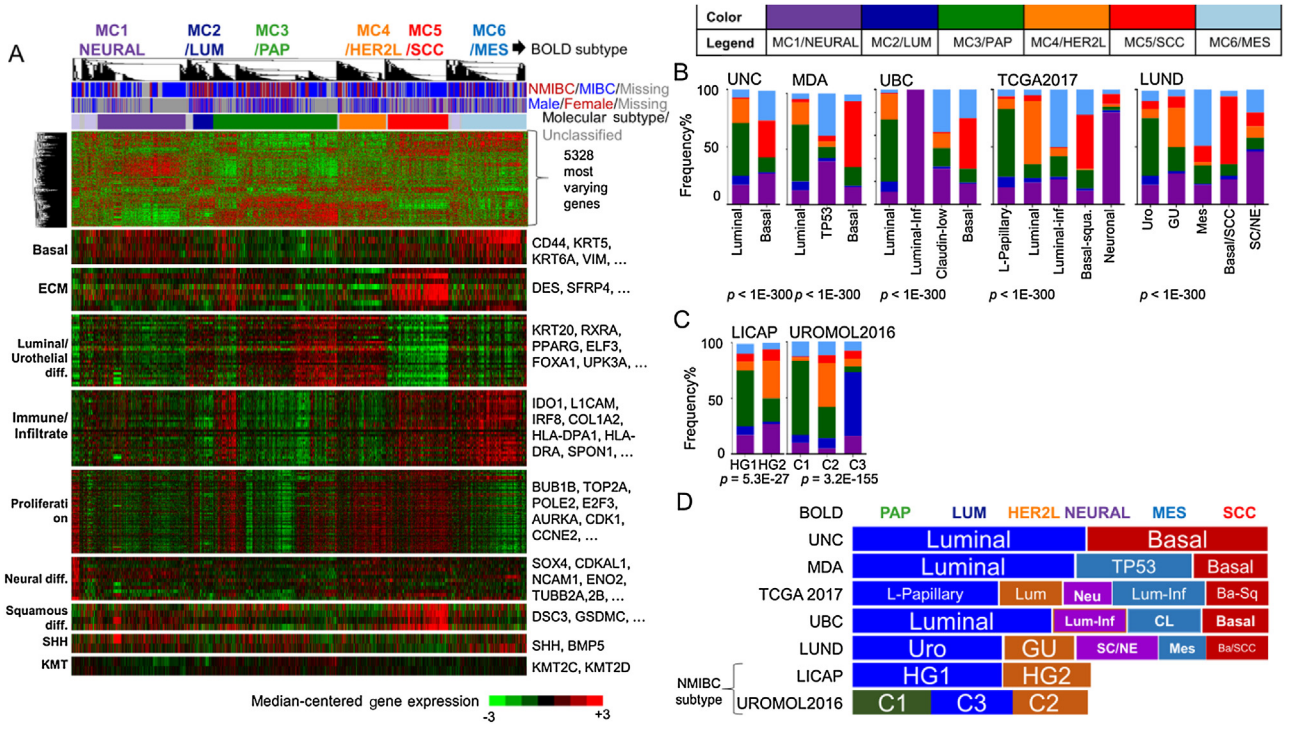

Fig. 1 – Unsupervised hierarchical clustering of urothelial carcinoma (UC) meta-cohort revealed six molecular subtypes. (A) Gene expression heatmap (red = high expression; green = low expression) of UC (*n* = 2411) aligned by identified molecular subtypes using 5328 most varying genes. Color bars show stage (NMIBC = red, MIBC = blue, grey = no annotation), and gender (female = red, male = blue, grey = no annotation). The subtypes are labeled as NEURAL (neural-like), LUM (luminal-like), PAP (papillary-like), HER2L (HER2-like), MES (mesenchymal-like), SCC (squamous-cell carcinoma-like), and denoted as BOLD (bladder carcinoma subtype of large meta-cohort database). Selected biomarkers for differentiation, proliferation are labeled. (B) Bar plots showing the frequency% (*y*-axis) association of BOLD with published molecular subtype: UNC, MDA, UBC, TCGA, and LUND. (C) Bar plots showing the frequency% (*y*-axis) of BOLD in the published NMIBC molecular subtypes of LICAP (left) [17], and UROMOL2016 [33] (right), using only the NMIBC found in BLCA meta-cohort. (D) A scheme depicting the inter-relationship between the BOLD and published molecular subtypes. The *p* values were computed by chi-square tests.
Color code: Purple = NEURAL; dark blue = LUM; green = PAP; orange = HER2L; red = SCC; light blue = MES.
Ba/SCC = basal/squamous-cell carcinoma-like; Ba-Sq = basal-squamous; BOLD = bladder carcinoma subtypes of large meta-cohort database; CL,= claudin-low; diff. = differentiation; ECM = extracellular matrix; GU = genomic unstable; HER2L, HER2-like; LICAP = Leeds Institute of Cancer and Pathology; L-papillary = luminal-papillary; Lum = luminal; LUM = luminal-like; Lum-inf = luminal infiltrated; LUND = Lund University; MDA = MD Anderson Cancer Center; Mes, mesenchymal; MES = mesenchymal-like; MIBC = muscle-invasive bladder carcinoma; Neu = neuronal; NEURAL = neural-like; NMIBC = non-muscle-invasive bladder cancer; PAP = papillary-like; SC/NE = small cell/neuroendocrine; TCGA = The Cancer Genome Atlas Network; UBC = University of British Columbia, UNC = University of North Carolina; Uro = urobasal.

Together, BOLD represents an umbrella subtype scheme capturing the various subtype schemes previously published.

3.2. *Both NMIBC and MIBC harbor BOLD subtypes, with distinct clinicopathological associations and pathways*

We next compared the characteristics of BOLD with those of the published subtypes it resembles. We applied silhouette analysis (Supplementary Fig. 6A; Supplementary data) to identify core samples for analyses of clinicopathological associations (Fig. 2; Table 2) and pathways. Unclassified samples or samples not associated with one of the BOLD subtypes were excluded from the analyses. In the entire BLCA meta-cohort, BOLD had different median overall survival (OS) outcomes ($p < 0.0001$; Fig. 2A): PAP (>135 mo), HER2L (107.7 mo), NEURAL, LUM, MES (~90 mo), and SCC (20.6 mo). The survival difference between PAP and LUM is most profound in NMIBC (Fig. 2A; middle panel). Intriguingly, the PAP subtype had a similar prognosis in MIBC (Fig. 2A; right panel), which may be due to the lower number of samples. Insufficient data did not allow an assessment of correlation with disease-free survival (Supplementary Fig. 6B). NEURAL, PAP, and SCC were significantly correlated to OS, and NEURAL, LUM, and MES were an independent prognostic factor (univariate and multivariate Cox regression analyses; Supplementary Table 10). The age at diagnosis was marginally different across BOLD, with the youngest age associated with the PAP subtype ($p = 0.0011$; Supplementary Fig. 6C). Interestingly, there were more females than males in the SCC subtype (Fig. 2B). LUM and PAP had more NMIBC, whereas NEURAL, MES, and SCC had more MIBC. HER2L had a comparable prevalence of NMIBC and MIBC. Interestingly, most Ta BLCAs were PAP, and T1 BLCAs were LUM and HER2L (Supplementary Fig. 6D; Table 2). Notably, ~20% of NMIBCs were NEURAL, MES, and SCC—subtypes predominantly comprising MIBC (Fig. 2B). Poor prognosis HER2L, MES, and SCC were characterized by late-stage ($p < 1E-300$), high-grade ($p = 3.3E-116$) cancers and were prone to lymph node invasion ($p = 6.2E-57$; Fig. 2B).

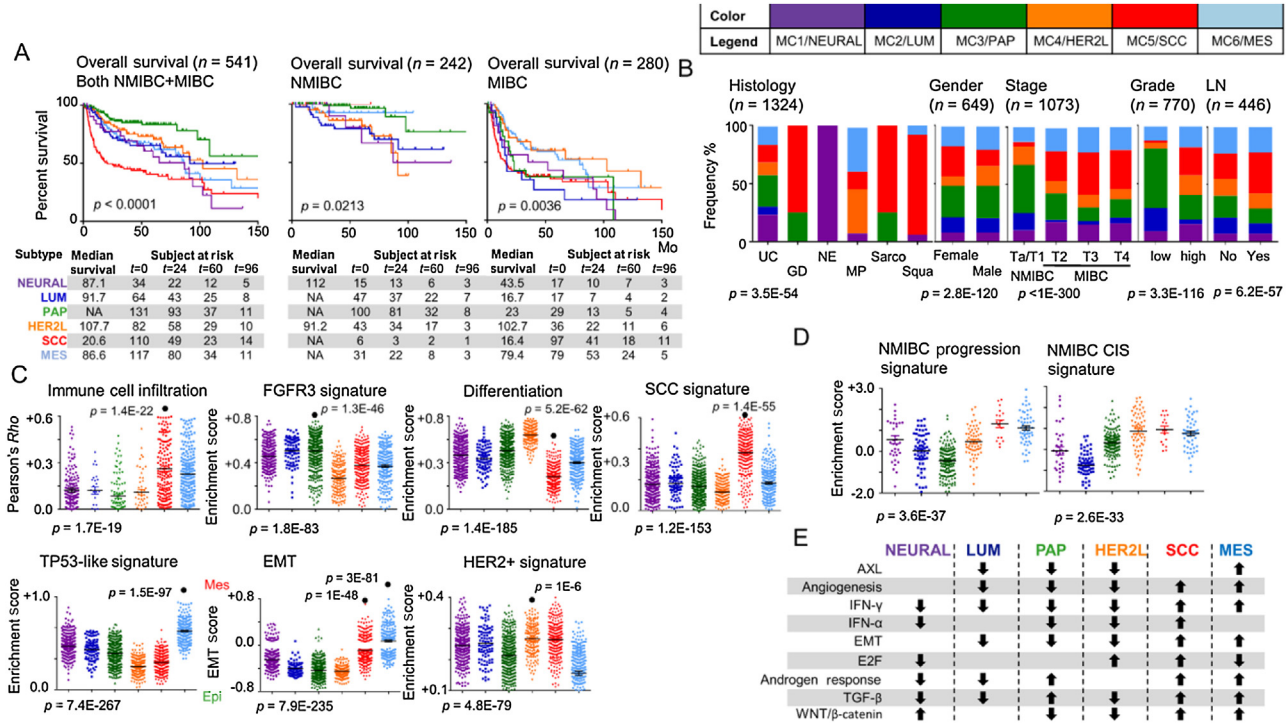

Fig. 2 – Characterization of BOLD. (A) Kaplan-Meier analysis of overall survival and BOLD in both NMIBC + MIBC (left), NMIBC only (middle), and MIBC (right). Median survival and subject at risks in months are given for each subtype. *T* denotes the time in months. Note that the summation of patients is not equal due to missing information of stage in certain patients. (B) Frequency% bar plot showing percentage of molecular subtype (*y*-axis) in different histology, gender, stage, grade, and lymph node/lymphovascular invasion) (*x*-axes). (C) Dot plot of immune cell infiltration, FGFR3 signature, Differentiation signature, Blaveri's SCC-like signatures, MDA TP53-like signature, EMT and breast cancer HER2+ subtype signature (*y*-axis) in BOLD (*x*-axis). Only core samples defined by silhouette width >0.01 were used for analysis. (D) Enrichment score (*y*-axis) of progression (left) and carcinoma in situ (right) in BOLD. The computation was performed only on NMIBC samples in BLCA meta-cohort. (E) Chart showing the elevated (up arrow) or depleted (down arrow) of selected pathways in BOLD. The *p* values were computed by log-rank (A), chi-square test (B), ANOVA (C, D; bottom) or Mann-Whitney (C; upper) tests. Data are presented as the mean ± SEM.
Color code: Purple = NEURAL; dark blue = LUM; green = PAP; orange = HER2L; red = SCC; light blue = MES.
ANOVA = analysis of variance; BOLD = bladder carcinoma subtypes of large meta-cohort database; CIS = carcinoma in situ; EMT = epithelial-mesenchymal transition; FGFR = fibroblast growth factor receptor; GD = glandular; HER2L, HER2-like; LN = lymph node; LUM = luminal-like; MES = mesenchymal-like; MIBC = muscle-invasive bladder cancer; MP = micro-papillary; NE = neuroendocrine; NEURAL = neural-like; NMIBC = non-muscle-invasive bladder cancer; PAP = papillary-like; Sarco = sarcomatoid; SCC = squamous-cell carcinoma-like; SEM = standard error of the mean; Squa = squamous; UC = urothelial cancer.

BLCAs of non-UC histologies are rare, aggressive, and have worse prognosis than UC (Supplementary Fig. 4A). Not surprisingly, the majority of non-UC histologies were distributed in the poor prognosis SCC and MES subtypes (Fig. 2B). The GD histology was mainly SCC; NE displayed similarity to NEURAL; MP was evenly distributed between HER2L and MES; and expectedly, BLCAs with Sarco and Squa differentiation were assigned primarily to SCC (Fig. 2B; Supplementary Table 5). Of note, LUM only had UC. This indicates that the rare variant histologies resembled transcriptomically the aggressive and poor prognosis subtypes of BOLD.

To ensure that the results presented were not biased by samples without complete clinical annotations (Table 1), we checked the distribution of clinicopathological parameters as well as the subtype in samples with annotation of histology, age, gender, stage, and grade available ($n = 802$), and samples without one or more of the annotation ($n = 1609$). Although there are differences in terms of distribution, all subtypes and clinicopathological parameters were represented in samples with or without complete clinical annotation (Supplementary Table 6). To affirm that the association results reported (Fig. 2; Supplementary Fig. 6C and 6D) were not an artefact arising from samples with missing data, we repeated the clinical association analyses using only core samples with complete annotation of histology, age, gender, stage, and grade ($n = 544$; Supplementary Fig. 6E–G; Supplementary Table 7). We observed that the subtype-clinicopathological parameters associations were highly concordant (Fig. 2B; Supplementary Fig. 6), demonstrating that the results were not distorted by the samples with incomplete clinical annotation.

From transcriptomic data, we observed higher infiltration of immune cells in MES and SCC subtypes. PAP is enriched for FGFR3 signature ($p = 1.3E-46$; Fig. 2C). The differentiation signature [34] showed that SCC was the most dedifferentiated ($p = 5.2E-62$). In concordance with the observation that MES is similar to the MDA_TP53 subtype, MES had the highest TP53-like signature ($p = 1.5E-97$; Fig. 2C). Likewise, SCC had the highest enrichment score for an SCC signature ($p = 1.4E-55$; Fig. 2C), and HER2L had the highest enrichment score of ERBB2+ signature [35]

Table 2 – Distribution of BOLD subtypes in selected clinicopathological parameters[a]

Parameter/subtype	*n*	NEU, *n* (%)	LUM, *n* (%)	PAP, *n* (%)	HER2L, *n* (%)	SCC, *n* (%)	MES, *n* (%)
Subtype prevalence	1543	350 (22.7)	89 (5.8)	422 (27.4)	170 (11)	268 (17.4)	244 (15.8)
Invasiveness							
NMIBC	424	38 (9)	64 (15.1)	175 (41.3)	70 (16.5)	17 (4)	60 (14.2)
MIBC	779	205 (26.3)	18 (2.3)	162 (20.8)	69 (8.9)	191 (24.5)	134 (17.2)
Stage							
Ta	209	17 (8.5)	24 (11.5)	122 (57.5)	14 (7)	9 (4)	23 (11.5)
T1 low-grade	75	11 (14.7)	24 (32)	24 (32)	5 (6.7)	0 (0)	11 (14.7)
T1 high-grade	113	10 (8.9)	9 (8.0)	25 (22.1)	44 (38.9)	6 (5.3)	19 (16.8)
T2	385	66 (17.1)	9 (2.3)	90 (23.4)	43 (11.2)	99 (25.7)	78 (20.3)
T3	173	26 (15)	5 (2.9)	21 (12.1)	19 (11)	64 (37)	38 (22)
T4	77	12 (15.6)	4 (5.2)	12 (15.6)	7 (9.1)	26 (33.8)	16 (20.8)
Lymph node invasion	72	6 (8.3)	6 (8.3)	9 (12.5)	9 (12.5)	26 (36.1)	16 (22.2)
Distant metastasis	47	3 (6.4%)	3 (6.4%)	11 (23.4%)	6 (12.8%)	15 (31.9%)	9 (19.1%)
Gender							
Female	150	12 (8.0%)	20 (13.3%)	41 (27.3%)	12 (8.0)	39 (26.0)	26 (17.3)
Male	499	42 (8.4)	60 (12.0)	139 (27.9)	87 (17.4)	71 (14.2)	100 (20.0)

HER2L = HER2-like; LUM = luminal-like; MES = mesenchymal-like; MIBC = muscle-invasive bladder carcinoma; NEU = neural-like; NMIBC = non–muscle-invasive bladder carcinoma; PAP = papillary-like; SCC = squamous-cell carcinoma-like.

[a] Percentage computation is based on a subset of core samples displaying the BOLD subtype only ($n \leq 1543$; silhouette width > 0.01), limited by the availability of clinical information (see column *n*). Please note that the number of samples with available clinical information is different from that of Table 1 due to our finer categorization of the clinical parameters. Only parameters related to invasiveness/staging were selected here.

(p = 1E-6; Fig. 2C). The EMT score is a value representing the position of a cell or a tumor in a spectrum ranging from the most epithelial (−1.0) to the most mesenchymal phenotype (+1.0) [31]; this score indicates that MES and SCC are more EMT than other subtypes (p = 3E-81 and 1E-48, respectively; Fig. 2C). Interestingly, MES and SCC showed enrichment of claudin-low breast cancer and basal signatures (Supplementary Fig. 7A; Supplementary data). MES was prone to co-occur with carcinoma in situ (CIS; p = 5.3E-37; Supplementary Fig. 6D; albeit, this was not conclusive [$n < 50$]). In addition, SCC, consistent with its high EMT characteristics (Fig. 2C), had greater propensity than the other subtypes to invade lymph node and to form distant metastasis (p = 4.9Ee-37; Table 2; Supplementary Fig. 6D). For BLCA treated by methotrexate, vinblastine, adriamycin, and cisplatin combination regimen, MES subtype samples were less likely to respond (p = 0.0109; Supplementary Fig. 6D). Looking at only NMIBC samples, consistently, MIBC-like subtypes NEURAL, SCC, and MES had higher enrichment of the progression signature [36] (Fig. 2D). Of note, LUM and HER2L—the more aggressive subtypes found in NMIBC—were significantly enriched for the progression signature (Fig. 2D). CIS signature [37] suggests that HER2L, SCC, and MES would be more likely to occur with CIS (Fig. 2D); the finding that HER2L and MES were likely to co-occur with CIS was concordant with clinical association (Supplementary Fig. 6D); however, SCC was not associated with CIS. Briefly, BOLD had different clinical outcomes and clinicopathological characteristics. Importantly, the distributions of good and poor prognosis subtypes were not exclusive to NMIBC or MIBC despite the prevalent differences.

Pathway analyses (Molecular Signature database version 6.1 [38]) revealed differential (increased) pathway enrichment across subtypes (Fig. 2D; Supplementary Table 11): WNT/β-catenin, neural-related pathways (GO axon, cranial-nerve, glial-cell) in NEURAL; MYC signaling in LUM; AXL signaling in MES; microtubule-related, ERBB signaling, DNA mismatch repair pathways in HER2L; androgen receptor (AR) signaling in PAP, MES, and SCC; wound healing pathway in more EMT subtypes NEURAL, MES, and SCC. TGF-β signaling in PAP, MES, and SCC; and EGF signaling in SCC. When comparing PAP and LUM—the two transcriptomically akin subtypes (Supplementary Table 12)—LUM had significantly higher MAPK activity, indicating LUM is a more proliferative form of PAP. Notably, PD1 and CTLA4 pathways were enriched in MES and SCC (Supplementary Table 11). Interferon-γ, angiogenesis, and inflammatory pathways were up-regulated in NEURAL, MES, and SCC. As several subtypes showed high immune cell infiltration and immune signature enrichment, we investigated if the BOLD classification results in differential immune cell infiltration allocation (Supplementary Table 13; Supplementary Fig. 7B). LUM has higher T-cell CD8+ infiltration, whereas MES and SCC have higher infiltration of tumor-associated macrophage M2 (Supplementary Fig. 7B). Because CD8+ cells are associated with anti-PD1 response [9], we projected a CD8 effector and a PD1 responder signature [39] (Supplementary Fig. 7C) and observed no significant correlation. Overall, BOLD recapitulated the existing published subtypes [10,11,13–15,21,30,40] and provided an elaborated classification of differential clinical outcomes.

3.3. *BOLD subtype stratification is reproducible in independent NMIBC, MIBC, and metastatic BLCA cohorts*

To examine the reproducibility of BOLD, we projected the subtype signatures derived using core samples (Supplementary Table 14; Supplementary data) on an NMIBC cohort (UROMOL), MIBC cohort (TCGA), and metastatic BLCA cohort (IMvigor210; Fig. 3A; Materials and methods). Of note, few samples in UROMOL were allocated to the NEURAL subtype. Subtype-clinicopathological associations were similar to those observed in the meta-cohort (Supplementary Fig. 8): PAP was associated with early-

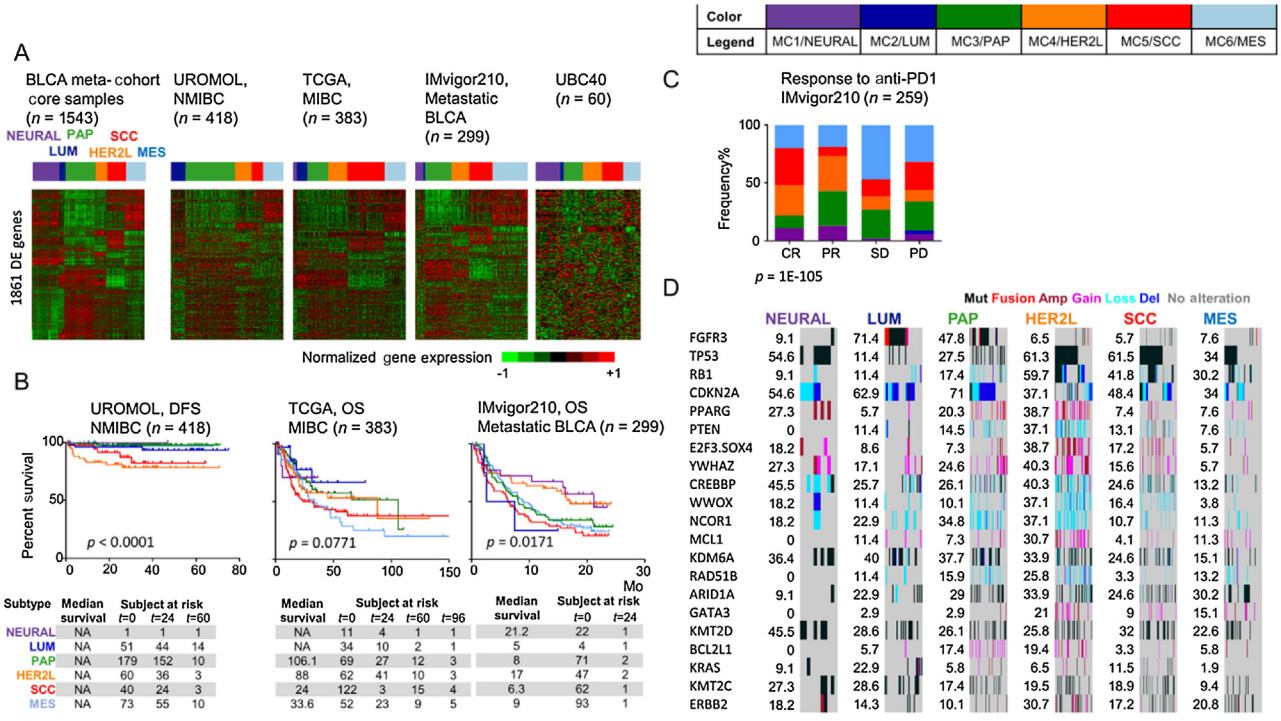

Fig. 3 – BOLD is reproducible in UROMOL, TCGA, and IMvigor210 cohorts. (A) Heatmap of 1861 most differentially expressed genes (red = high expression, green = low expression) across BOLD in core samples (silhouette width > 0.01) in BLCA meta-cohort, and in NMIBC cohort UROMOL, MIBC cohort TCGA, metastatic BLCA cohort IMvigor210, and cell lines UBC40. Color bars above heatmap show the inferred BOLD subtype on the different cohorts. (B) Kaplan-Meier analyses of OS and DFS (progression- and recurrence-free) in UROMOL (left), TCGA (middle), and IMvigor210 (right). (C) Frequency% (*y*-axis) plot of response to anti-PD1 (atezolizumab). Response is measured by RECIST v1.1 (*x*-axis). (D) Heatmap of BLCA significantly mutated genes and focal copy number aberrations differentially associated with subtypes. Copy number (*cn*) definition in log2 ratio: Amp, $cn > 1$; gain, $0.59 < cn \leq 1$; loss, $-1 \leq cn < -0.42$; del, $cn < -1$. The frequency% of altered genes in each subtype is given next to the heatmap.
The *p* values were computed by log-rank test (B) and ANOVA (C).
Color code: Purple = NEURAL; dark blue = LUM; green = PAP; orange = HER2L; red = SCC; light blue = MES; black = mutated; maroon = amp; pink = gain; light blue = loss; dark blue = del.
ANOVA = analysis of variance; Amp = copy number amplification; BLCA = bladder carcinoma; BOLD = bladder carcinoma subtypes of large meta-cohort database; CR = complete response; Del = copy number deletion; DFS = disease-free survival; HER2L = HER2-like; LUM = luminal-like; MES = mesenchymal-like; MIBC = muscle-invasive bladder cancer; Mut = mutated; NEURAL = neural-like; NMIBC = non-muscle-invasive bladder cancer; OS = overall survival; PAP = papillary-like; PD = progressive disease; PR = partial response; SCC = squamous-cell carcinoma-like; SD = stable disease; TCGA = The Cancer Genome Atlas; UBC 40 cell line = urothelial bladder cancer 40 cell line.

stage, low-grade, lower European Organisation for Research and Treatment of Cancer scores, smaller (<3 cm) tumors, and younger patients; SCC tended to progress during treatment (Supplementary Fig. 8D). Intriguingly, the observation that PAP had a good prognosis in NMIBC but comparable prognosis to that of other subtypes in MIBC was replicated in UROMOL, TCGA, and IMvigor210 cohorts (Fig. 3B). This suggests that PAP classification is more relevant in NMIBC, where PAP NMIBC and non-PAP NMIBC showed significantly different OS (Supplementary Fig. 8B; $p = 0.0022$). Nevertheless, we observed that SCC had the poorest outcome across NMIBC, MIBC, and metastatic BLCA. Similarly, LUM and MES both performed poorly in terms of survival. HER2L had a similar poor survival outcome in NMIBC and MIBC but relatively better prognosis in an anti-PD1-treated cohort in IMvigor210. This could be because HER2L is more likely to respond to anti-PD1 treatment (Fig. 3C). Higher mutation, copy number aberrations, and neoantigen load, thus, may predict the response to anti-PD1 treatment (Supplementary Fig. 9). In general, the clinical characterization of BOLD in our BLCA meta-cohort, UROMOL, TCGA, and IMvigor210 cohorts were concordant, indicating good reproducibility of our subtype identification.

Using TCGA data, we investigated the association of BOLD with significantly mutated genes, focal [11] and genome-wide copy number profiles (Fig. 3D; Supplementary Fig. 9C; Supplementary Table 16). Similar to previous reports, we observed that *FGFR3* fusion, mutation, and amplification were highly enriched in PAP, and that *TP53* mutation was enriched in HER2L and SCC. HER2L had more mutations, copy number aberrations, and neoantigen load (Supplementary Fig. 9A). Notably, PAP and LUM had 9q extensive deletions (Supplementary Fig. 9C), mimicking the low-risk HG1 NMIBC genomic subtype [17] but had different prognosis outcomes. In brief, BOLD exhibited diverse genetic and genomic alterations that may point to a potential targeted therapy.

We noticed that BLCA tumors harbor subtype-specific actionable mutations, aberrations, or pathway activations (Supplementary Tables 11 and 16): *FGFR3-TACC3* fusion in PAP; *ERBB2* amplification in HER2L and LUM (Supplementary

Table 16; Supplementary Fig. 10A; Supplementary data); *AXL* pathway in MES; AR pathway in MES and SCC; PD1 and CTLA4 pathways in MES and SCC; and *PPARG* fusion/amplification in HER2L. Of note, high *PPARG* and *MRE11* expressions have been linked to good outcome to bladder-preserving trimodality treatment (maximal transurethral resection, radiotherapy, and chemotherapy or immunotherapy) [41], suggesting HER2L could be a good candidate for trimodality treatment (Supplementary Fig. 10B). To explore a potential treatment strategy, we projected the BOLD signature to a BLCA cell line collection, UBC40 [42] (Supplementary Table 17), a patient-derived organoid collection GSE103990 [43] established from mainly Ta/T1 BLCA, and BLCA cell lines from COSMIC [44]. We correlated subtype enrichment scores with 50% growth inhibitory concentration (GI50) of different compounds. The epithelial-like PAP and LUM were more resistant than SCC (Supplementary Fig. 10C–E). MES, being stem-like, is expectedly resistant. HER2L, being genomically unstable, surprisingly shows no preferential sensitivity or resistance to any of the compounds tested (Supplementary data). In summary, BOLD subtypes have distinct molecular characteristics that are targetable, and the preliminary cell line-drug response analysis shows that subtypes have differential responses to compounds.

4. Discussion

Molecular subtyping holds great promise in understanding disease and in personalized therapeutics. In BLCA, an endeavor has been made to classify the disease into molecular subtypes to guide disease management [10,11,13–15,30,40]. However, most studies to date have been based on smaller cohort sizes (100–500 samples) even though >3000 BLCA samples are required to reliably detect gene mutations in 2% of samples [40]. Accordingly, more samples are needed to detect subtype differences with greater statistical power and to identify rare subtypes. This is exemplified by the TCGA, where only four gene expression subtypes were detected among 130 samples initially and later refined to five after expanding to 412 samples [10,11]. Here, we curated a database of >2400 samples and identified six molecular subtypes (denoted as BOLD). These six subtypes showed good concordance with previous reports, thus representing a convergence of findings. A recent meeting reached a consensus that there is a basal/SCC subtype; however, it remains unclear whether luminal/urobasal subtypes should be considered [19]. By amalgamating a large dataset, our findings not only affirm the basal/SCC subtype but also corroborate the existence of three luminal/epithelial-like subtypes (PAP, LUM, HER2L), a NEURAL subtype, and a claudin-low/stem-like MES subtype. Furthermore, our study showed that ~20% of NMIBCs display features of MIBC-like subtypes such as MES and SCC. Analysis of the meta-cohort also revealed that the rare but aggressive variant histologies of BLCA showed transcriptomic similarity with poor prognosis subtypes—SCC, MES, and HER2L. This resonates with the findings that NE BLCA has striking resemblance with UC [45], exhibiting similar mutational landscape and signature. However, a caveat of the rare histology analysis is the low number of samples for each variant ($n < 50$), and that the rare variants often co-existed with UC within a tumor lesion.

Molecular characterization of BOLD uncovered specific exploitable vulnerabilities. Notably, PAP NMIBC patients have significantly better survival outcomes and may, thus, require less frequent surveillance. HER2L, LUM, MES, and SCC are at high risk of progression and would, therefore, require more frequent monitoring and may be treated more aggressively. It is not surprising that BOLD displayed widely preferential responses. From a cell line-drug response analysis, MES was generally resistant to chemotherapy compounds, such as cisplatin and paclitaxel, agreeing with a previous report that claudin-low (resembles MES) tumors are less likely to respond to cisplatin-neoadjuvant chemotherapy [13]. While NEURAL, MES, and SCC had elevated PD1 and CTLA4 signaling, suggesting that they may be candidates for anti-PD(L)1 or anti-CTLA4 treatments; data from IMvigor210 show that the three subtypes were not significantly associated with complete response, with MES being the least beneficial. However, HER2L had a high tumor mutational burden and neoantigen load, which are associated or predicted with durable immune checkpoint inhibition response [8,9]. IMvigor210 data show that HER2L is more likely to be benefited from anti-PD(L)1 treatment. Interestingly, HER2L displayed elevated DNA-replication/cell-cycle signaling, lower hypoxia signaling (Supplementary Table 11), and at the same time high *PPARG* and *MRE11* expression (Fig. 1A; Supplementary Fig. 10B), suggesting that HER2L tumors may benefit from bladder-preserving trimodality therapy (maximal transurethral resection, followed by concurrent radiotherapy and chemotherapy/immunotherapy) [41,46]. However, BLCA is heterogeneous and unlikely to be solely dependent on one pathway. For example, MES and SCC, despite having high PD1, CTLA-4 signaling, also exhibited elevated angiogenesis, TGF-β signaling, and increased infiltration of immunosuppressive macrophage M2, which have been linked to lack of immunotherapy response [9]. Thus, a single-agent approach may not yield significant outcome improvement in these subtypes. Instead, combining immune checkpoint inhibition with an AXL inhibitor [47] in MES, an anti-TGF-β in MES and SCC [9], or an AR inhibitor in MES, and SCC may be viable treatment options [3]. Other targetable axes that could be explored include: (1) *FGFR3* amplification, activating mutations, and *FGFR3-TACC3* fusion in MIBC or metastatic BLCA of PAP subtype through the use of a pan-FGFR inhibitor [5]; TCGA luminal-papillary subtype, which resembling PAP, was shown to have promising activity to a pan-FGFR inhibitor Erdafitinib [48], suggesting the feasibility of targeting FGFR3 in PAP subtype, (2) ERBB2 amplification in HER2L and LUM via a HER2 inhibitor, (3) PPARG activating mutation, fusion in HER2L by a PPARG inhibitor [49], and (4) *PTGS2*-driven wound healing pathway in NEURAL, MES, and SCC via a COX2 inhibitor [50]. Supplementary Figure 11 summarizes the potential therapeutic framework of BOLD stratification.

As this study is based on curation and re-analysis of samples from different sources, the study is limited by the completeness, accuracy, or quality of the samples collected. More of the available studies were MIBC-focused, and thus, the prevalence and natural history of BLCA were not fully represented by the compiled meta-cohort. In addition, the main limitations of our study are the lack of clinical annotation among several publicly available BLCA cohorts. Therefore, while care has been taken to ensure that the analyses were not biased by samples without complete clinical annotation (Supplementary Tables 6 and 7), we cannot rule out the possibility of misdiagnosis, especially for Ta/T1 and CIS cases. However, we believe even such misdiagnosed or wrongly annotated cases are likely rare, and the effect of such cases within >2400 cohort should be minimal. Another limitation is that some genes were not available in the meta-cohort as the analysis required a comparison across different gene expression quantification technologies. However, the effect of missing genes should be negligible in regard to subtype prediction, as seen by the good molecular characteristic conformity of the BOLD classification with other published subtypes. Finally, the clinical relevance of these six molecular subtypes is based on survival data analysis. The therapeutic impact of these subtypes could not be assessed due to the unavailability of treatment-related data.

5. Conclusions

BLCA can be stratified into six molecular subtypes, each with distinct pathways and targetable vulnerability. These findings may have relevance in clinical practice. Therapeutic implications should be evaluated in prospective biomarker-driven clinical trials.

Author contributions: Tuan Zea Tan, Ruby Yun-Ju Huang, and Jean-Paul Thiery had full access to all the data in the study and take responsibility for the integrity of the data and the accuracy of the data analysis.

Study concept and design: T.Z. Tan, Thiery.
Acquisition of data: T.Z. Tan.
Analysis and interpretation of data: T.Z. Tan, Rouanne, K.T. Tan, Huang, Thiery.
Drafting of the manuscript: T.Z. Tan, Rouanne, Thiery.
Critical revision of the manuscript for important intellectual content: T.Z. Tan, Rouanne, K.T. Tan, Huang, Thiery.
Statistical analysis: T.Z. Tan.
Obtaining funding: Huang.
Administrative, technical, or material support: T.Z. Tan.
Supervision: Huang, Thiery.
Other: None.

Financial disclosures: Tuan Zea Tan, Ruby Yun-Ju Huang, and Jean-Paul Thiery certify that all conflicts of interest, including specific financial interests and relationships and affiliations relevant to the subject matter or materials discussed in the manuscript (eg, employment/affiliation, grants or funding, consultancies, honoraria, stock ownership or options, expert testimony, royalties, or patents filed, received, or pending), are the following: K.T. Tan is an employee of ACT Genomic. J.-P. Thiery is a consultant/advisory board member for Aim Biotech Singapore, ACT Genomic and CSO BioCheetah Ltd Singapore. No potential conflicts of interest were disclosed by the other authors.

Funding/Support and role of the sponsor: None.

Acknowledgments: This work is supported by National Research Foundation (NRF) Singapore and the Singapore Ministry of Education under its Research Centres of Excellence initiative to R.H.; National Medical Research Council (NMRC) under its Centre Grant scheme to National University Cancer Institute (NCIS) to R.H.

Appendix A. Supplementary data

Supplementary data associated with this article can be found, in the online version, at https://doi.org/10.1016/j.eururo.2018.08.027.

References

[1] Torre LA, Bray F, Siegel RL, Ferlay J, Lortet-Tieulent J, Jemal A. Global cancer statistics, 2012. CA Cancer J Clin 2015;65:87–108.
[2] Sanli O, Dobruch J, Knowles MA, et al. Bladder cancer. Nat Rev Dis Primers 2017;3:17022.
[3] Knowles MA, Hurst CD. Molecular biology of bladder cancer: new insights into pathogenesis and clinical diversity. Nat Rev Cancer 2015;15:25–41.
[4] Witjes JA, Lebret T, Comperat EM, et al. Updated 2016 EAU Guidelines on muscle-invasive and metastatic bladder cancer. Eur Urol 2017;71:462–75.
[5] Tabernero J, Bahleda R, Dienstmann R, et al. Phase I dose-escalation study of JNJ-42756493, an oral pan-fibroblast growth factor receptor inhibitor, in patients with advanced solid tumors. J Clin Oncol 2015;33:3401–8.
[6] Rouanne M, Loriot Y, Lebret T, Soria JC. Novel therapeutic targets in advanced urothelial carcinoma. Crit Rev Oncol Hematol 2016;98:106–15.
[7] Powles T, Eder JP, Fine GD, et al. MPDL3280A (anti-PD-L1) treatment leads to clinical activity in metastatic bladder cancer. Nature 2014;515:558–62.
[8] Rosenberg JE, Hoffman-Censits J, Powles T, et al. Atezolizumab in patients with locally advanced and metastatic urothelial carcinoma who have progressed following treatment with platinum-based chemotherapy: a single-arm, multicentre, phase 2 trial. Lancet 2016;387:1909–20.
[9] Mariathasan S, Turley SJ, Nickles D, et al. TGFbeta attenuates tumour response to PD-L1 blockade by contributing to exclusion of T cells. Nature 2018;554:544–8.
[10] Cancer Genome Atlas Research N. Comprehensive molecular characterization of urothelial bladder carcinoma. Nature 2014;507:315–22.
[11] Robertson AG, Kim J, Al-Ahmadie H, et al. Comprehensive molecular characterization of muscle-invasive bladder cancer. Cell 2017;171:540–56, e25.
[12] Rebouissou S, Bernard-Pierrot I, de Reynies A, et al. EGFR as a potential therapeutic target for a subset of muscle-invasive bladder cancers presenting a basal-like phenotype. Sci Transl Med 2014;6:244ra91.
[13] Seiler R, Ashab HAD, Erho N, et al. Impact of molecular subtypes in muscle-invasive bladder cancer on predicting response and survival after neoadjuvant chemotherapy. Eur Urol 2017;72:544–54.
[14] Sjodahl G, Lauss M, Lovgren K, et al. A molecular taxonomy for urothelial carcinoma. Clin Cancer Res 2012;18:3377–86.
[15] Choi W, Porten S, Kim S, et al. Identification of distinct basal and luminal subtypes of muscle-invasive bladder cancer with different sensitivities to frontline chemotherapy. Cancer Cell 2014;25:152–65.

[16] Aine M, Eriksson P, Liedberg F, Sjödahl G, Höglund M. Biological determinants of bladder cancer gene expression subtypes. Sci Rep 2015;5:10957.
[17] Hurst CD, Alder O, Platt FM, et al. Genomic subtypes of non-invasive bladder cancer with distinct metabolic profile and female gender bias in KDM6A mutation frequency. Cancer Cell 2017;32:701–15, e7.
[18] Aine M, Eriksson P, Liedberg F, Höglund M, Sjödahl G. On molecular classification of bladder cancer: out of one, many. Eur Urol 2015;68:921–3.
[19] Lerner SP, McConkey DJ, Hoadley KA, et al. Bladder cancer molecular taxonomy: summary from a consensus meeting. Bladder Cancer 2016;2:37–47.
[20] Choi W, Ochoa A, McConkey DJ, et al. Genetic alterations in the molecular subtypes of bladder cancer: illustration in the Cancer Genome Atlas Dataset. Eur Urol 2017;72:354–65.
[21] Sjodahl G, Eriksson P, Liedberg F, Höglund M. Molecular classification of urothelial carcinoma: global mRNA classification versus tumour-cell phenotype classification. J Pathol 2017;242:113–25.
[22] Ein-Dor L, Kela I, Getz G, Givol D, Domany E. Outcome signature genes in breast cancer: is there a unique set? Bioinformatics 2005;21:171–8.
[23] McConkey DJ, Choi W. Subtyping bladder cancers: biology vs bioinformatics. J Natl Cancer Inst 2018;110:439–40.
[24] George SL. Reducing patient eligibility criteria in cancer clinical trials. J Clin Oncol 1996;14:1364–70.
[25] Santos M, Martinez-Fernandez M, Duenas M, et al. In vivo disruption of an Rb-E2F-Ezh2 signaling loop causes bladder cancer. Cancer Res 2014;74:6565–77.
[26] Johnson WE, Li C, Rabinovic A. Adjusting batch effects in microarray expression data using empirical Bayes methods. Biostatistics 2007;8:118–27.
[27] Shabalin AA, Tjelmeland H, Fan C, Perou CM, Nobel AB. Merging two gene-expression studies via cross-platform normalization. Bioinformatics 2008;24:1154–60.
[28] Center BITGDA. Firehose stddata_2016_01_28 run. Broad Institute of MIT and Harvard; 2016.
[29] Wilkerson MD, Hayes DN. ConsensusClusterPlus: a class discovery tool with confidence assessments and item tracking. Bioinformatics 2010;26:1572–3.
[30] Damrauer JS, Hoadley KA, Chism DD, et al. Intrinsic subtypes of high-grade bladder cancer reflect the hallmarks of breast cancer biology. Proc Natl Acad Sci U S A 2014;111:3110–5.
[31] Tan TZ, Miow QH, Miki Y, et al. Epithelial-mesenchymal transition spectrum quantification and its efficacy in deciphering survival and drug responses of cancer patients. EMBO Mol Med 2014;6:1279–93.
[32] Newman AM, Liu CL, Green MR, et al. Robust enumeration of cell subsets from tissue expression profiles. Nat Methods 2015;12:453–7.
[33] Hedegaard J, Lamy P, Nordentoft I, et al. Comprehensive transcriptional analysis of early-stage urothelial carcinoma. Cancer Cell 2016;30:27–42.
[34] Mo Q, Nikolos F, Chen F, et al. Prognostic power of a tumor differentiation gene signature for bladder urothelial carcinomas. J Natl Cancer Inst 2018;110:448–59.
[35] Prat A, Parker JS, Karginova O, et al. Phenotypic and molecular characterization of the claudin-low intrinsic subtype of breast cancer. Breast Cancer Res 2010;12:R68.
[36] Dyrskjot L, Reinert T, Algaba F, et al. Prognostic impact of a 12-gene progression score in non-muscle-invasive bladder cancer: a prospective multicentre validation study. Eur Urol 2017;72:461–9.
[37] Dyrskjot L, Kruhoffer M, Thykjaer T, et al. Gene expression in the urinary bladder: a common carcinoma in situ gene expression signature exists disregarding histopathological classification. Cancer Res 2004;64:4040–8.
[38] Subramanian A, Tamayo P, Mootha VK, et al. Gene set enrichment analysis: a knowledge-based approach for interpreting genome-wide expression profiles. Proc Natl Acad Sci U S A 2005;102:15545–50.
[39] Hugo W, Zaretsky JM, Sun L, et al. Genomic and transcriptomic features of response to anti-PD-1 therapy in metastatic melanoma. Cell 2016;165:35–44.
[40] Hurst CD, Knowles MA. Bladder cancer: multi-omic profiling refines the molecular view. Nat Rev Clin Oncol 2018;15:203.
[41] Miyamoto DT, Gibb E, Mouw KW, et al. Genomic profiling of muscle invasive bladder cancer to predict response to bladder-sparing trimodality therapy. Genitourinary Cancers Symposium. San Francisco: ASCO; 2018,. http://ascopubs.org/doi/abs/10.1200/JCO.2018.36.6_suppl.513
[42] Lee JK, Havaleshko DM, Cho H, et al. A strategy for predicting the chemosensitivity of human cancers and its application to drug discovery. Proc Natl Acad Sci U S A 2007;104:13086–91.
[43] Lee SH, Hu W, Matulay JT, et al. Tumor evolution and drug response in patient-derived organoid models of bladder cancer. Cell 2018;173:515–28, e17.
[44] Yang W, Soares J, Greninger P, et al. Genomics of Drug Sensitivity in Cancer (GDSC): a resource for therapeutic biomarker discovery in cancer cells. Nucleic Acids Res 2013;41:D955–61.
[45] Shen P, Jing Y, Zhang R, et al. Comprehensive genomic profiling of neuroendocrine bladder cancer pinpoints molecular origin and potential therapeutics. Oncogene 2018;37:3039–44.
[46] Hoskin P. Use of molecular markers in bladder preservation. Genitourinary Cancers Symposium. San Francisco, CA: ASCO; 2018.
[47] Antony J, Tan TZ, Kelly Z, et al. The GAS6-AXL signaling network is a mesenchymal (Mes) molecular subtype-specific therapeutic target for ovarian cancer. Sci Signal 2016;9:ra97.
[48] Siefker-Radtke AO, Necchi A, Park SH, et al. First results from the primary analysis population of the phase 2 study of erdafitinib (ERDA; JNJ-42756493) in patients (pts) with metastatic or unresectable urothelial carcinoma (mUC) and FGFR alterations (FGFRalt). Chicago, IL: ASCO; 2018,. http://ascopubs.org/doi/abs/10.1200/JCO.2018.36.15_suppl.4503
[49] Goldstein JT, Berger AC, Shih J, et al. Genomic activation of PPARG reveals a candidate therapeutic axis in bladder cancer. Cancer Res 2017;77:6987–98.
[50] Kurtova AV, Xiao J, Mo Q, et al. Blocking PGE2-induced tumour repopulation abrogates bladder cancer chemoresistance. Nature 2015;517:209–13.